# [3+2] Cycloadditions and Retro-cycloadditions of Niobium Imido Complexes: An Experimental and Computational Mechanistic Study

*Anukta Jain,[†] Jade I. Fostvedt,[†] Benjamin M. Kriegel, David W. Small, Lauren N. Grant, Robert G. Bergman, and John Arnold**

Department of Chemistry, University of California, Berkeley, CA, 94720, United States

[†]These authors contributed equally to the work.

ABSTRACT. We demonstrate reactivity between a β-diketiminate-supported niobium(III) imido complex and alkyl azides to form niobatetrazene complexes (BDI)Nb(N$^t$Bu)(RNNNNR) (BDI = *N*,*N*-bis(2,6-diisopropylphenyl)-3,5-dimethyl-β-diketiminate; R = cyclohexyl (**1**), benzyl (**2**)). Intriguingly, niobatetrazene complexes **1** and **2** can be interconverted *via* addition of the appropriate alkyl azide, likely through a series of concerted [3+2] cycloaddition and retrocycloaddition reactions in which π-loaded bis(imido) intermediates are formed. The bis(imido) intermediates were trapped upon addition of alkyl isocyanides to yield five-coordinate bis(imido) complexes (BDI)Nb(N$^t$Bu)(NCy)(CNR) (R = *tert*-butyl (**4a**), cyclohexyl (**4b**)). Two computational methods—density functional theory (DFT) and density functional tight binding (DFTB)—were employed to calculate the lowest energy pathway across the potential energy surface for this multistep transformation. Reaction path calculations for individual cycloaddition

or retrocycloaddition processes along the multistep reaction pathway showed that these transformations occur *via* a concerted, yet highly asynchronous mechanism, in which the two bond-breaking or -making events do not occur simultaneously. The use of the DFTB method in this work highlights its advantages and utility for studying transition metal systems.

## Introduction

Early transition metal (ETM; groups 3-5) complexes bearing imido ligands have long intrigued the organometallic community due to their diverse reactivity with both saturated and unsaturated substrates.[1-4] Such complexes gained attention for their reactivity in 1988, when both Bergman and Wolczanski reported the seminal examples of C-H activation mediated by Zr imido complexes, back-to-back in the same journal issue.[5,6] Since then, the ETM-nitrogen double bond has been demonstrated to engage in rich chemistry, including cycloaddition with unsaturated bonds,[4,7-9] 1,2-addition of a variety of small molecules,[3,10] and imido group transfer.[11] Several noteworthy examples of catalytic transformations leveraging reactive ETM imido groups have also been reported, such as *Z*-selective semihydrogenation of alkynes,[12,13] pyrrole formation,[14-16] hydroamination,[17-19] carboamination of alkynes,[20-24] and imine metathesis.[25-29]

The majority of these stoichiometric and catalytic processes rely on pericyclic reactions, most commonly [2+2] cycloadditions, between unsaturated substrates and ETM-imidos.[4,8,9] While examples of [2+2] and [4+2] cycloadditions across ETM imido groups are legion,[4,7-9,17-30] there are far fewer reports of [3+2] cycloadditions (also known as 1,3-dipolar additions) across ETM imido groups. These pericyclic reactions occur between a 1,3-dipole—usually an alkyl or aryl azide—and an ETM-imido *via* a concerted, often asynchronous, symmetry-allowed pathway.[31-33] Stoichiometric [3+2] cycloadditions of ETM imido groups with organic azides in the forward direction yield metallatetrazene complexes (reports exist for Zr,[34,35] Nb,[36] and Th[37-39]), and a few

of these complexes undergo subsequent retro-[3+2]-cycloaddition,[34,36,37] including Bergman's imidozirconocene-mediated azide metathesis.[35]

It is interesting to note that cycloadditions ([2+2], [2+4], and [3+2]) involving ETMs are largely mediated by high valent group 3 and 4 mono(imido) complexes or group 5 bis(imido) complexes, whereas reports of group 5 mono(imido)-mediated cycloadditions are rare.[29,40-42] This observation can be attributed to increasing covalency of the bonding interaction between the metal $d_\pi$ and imido 2p orbitals upon moving from groups 3 to 5, resulting in less polar, less reactive imido moieties for the group 5 transition metals.[43] Our group and others have shown that reactivity of group 5 imido complexes can be enhanced by the addition of a second imido group, which serves to electronically saturate the symmetrically available π-bonding orbitals on the metal, leading to increased polarization and reactivity at one of the two imido groups; this strategy is known as π-loading.[12,16,30,44-50] We recently reported several BDI-supported Nb(V) bis(imido) complexes (BDI = *N*,*N*-bis(2,6-diisopropylphenyl)-3,5-dimethyl-β-diketiminate) that were active toward 1,2-addition,[48] [2+2] cycloaddition,[48,30] nitrene metathesis, and catalytic nitrene transfer.[45] We have also demonstrated stoichiometric [3+2] cycloaddition reactivity between a Nb bis(imido) complex and *tert*-butyl azide.[36]

Here, we report reactions of a Nb(III) mono(imido) complex, (BDI)Nb(N$^t$Bu)($\eta^6$-$C_6H_6$), with various alkyl azides to form niobatetrazene complexes. We show that these niobatetrazene complexes can be interconverted upon addition of excess alkyl azide. This transformation occurs *via* a series of [3+2] and retro-[3+2]-cycloaddition reactions and generates two π-loaded bis(imido) intermediates. This multi-step reaction pathway was subjected to rigorous computational analysis using Density Functional Theory (DFT) and a recently introduced variant of Density Functional Tight Binding (DFTB), called GFN2-xTB.[51] DFTB allows for significant savings in computational

time, while retaining some basic quantum mechanical characteristics of DFT. We compare the accuracy of these two approaches and gain insights into the asynchronous nature of these concerted cycloaddition and retrocycloaddition reactions.

## Results and Discussion

*Synthesis and Azide Metathesis Reactivity of Niobatetrazene Complexes.*

The low-valent Nb(III) complex (BDI)Nb(N$^t$Bu)($\eta^6$-$C_6H_6$) (BDI = *N*,*N*'-bis(2,6-diisopropylphenyl)-3,5-dimethyl-β-diketiminate) reacts with two equivalents of alkyl azides $RN_3$ (R = Cy, Bn) to give niobatetrazene complexes **1** (R = Cy) and **2** (R = Bn) as red crystals in 77% or 33% yield, respectively (Scheme 1). Formation of compounds **1** and **2** likely resulted from initial nitrene transfer to form Nb(V) bis(imido) intermediates **A** and **B** (Scheme 1),[45] followed by [3+2] cycloaddition of a second equivalent of azide. Related group 4, 5, and 6 tetrazene complexes have been accessed from [3+2] cycloadditions of azides across imido groups.[7,30,35,52-54] The $^1$H NMR spectra of both **1** and **2** are consistent with $C_s$ symmetry in solution (Figures S1 and S3, respectively). A minor side product (*ca.* 10% relative to **2**) can be observed in the $^1$H NMR spectrum of **2**; repeated recrystallizations did not change the relative ratio of these two species. Elemental analysis indicates that **2** is quite pure; as such, we posit this minor species is the product of cycloaddition across the *tert*-butyl imido group, (BDI)Nb(NBn)($^t$BuNNNNBn), which would possess the same elemental composition as **2**.

**Scheme 1.** Syntheses of compounds **1** and **2**, and conversion between the two products *via* compound **3**.

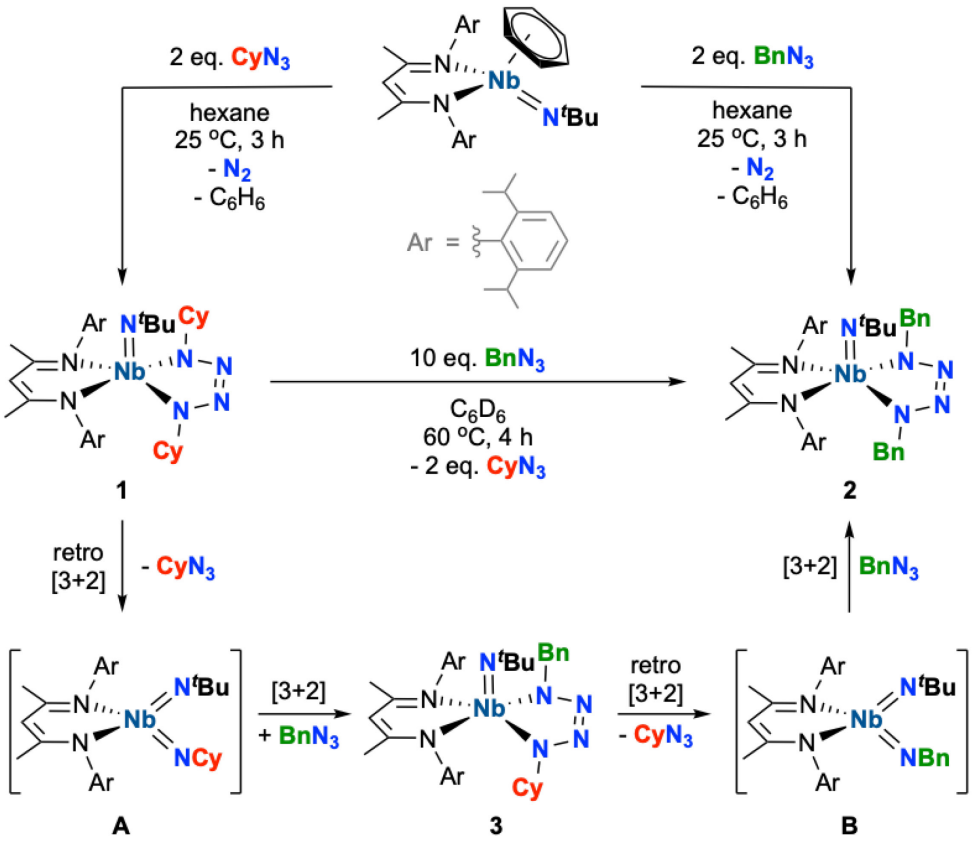


Compounds **1** and **2** were also characterized by X-ray crystallography (Figure 1 and Table S2, ESI). Complex **1** exhibits nearly ideal square-based pyramidal ($\tau_5 = 0.01$)[55] geometry at the metal center with the imido group occupying the apical position, resulting in a solid-state structure with only slight distortions from its $C_s$ solution symmetry. The benzyl derivative **2** exhibits distorted square-based pyramidal geometry ($\tau_5 = 0.13$) with one of the BDI nitrogen atoms occupying the apical position. Hence, **2** displays $C_1$ symmetry in the solid state, in contrast to its $C_s$ solution symmetry. Comparison of the metrical parameters between the two crystal structures suggests that **1** is more sterically crowded than **2**: the average Nb–N(BDI) bond lengths in **1** are longer than those in **2** by 0.080(4) Å, while the average differences in Nb–N(tetrazene) bond lengths are less dramatic (Table S2). We posit that steric clashing between tetrazene cyclohexyl groups and BDI

2,6-diisopropylphenyl groups (which sit above and below the cyclohexyl groups) in **1** locks this complex into a nearly ideal square-based pyramidal geometry, while tetrazene benzyl groups in **2** are oriented away from BDI 2,6-diisopropylphenyl groups, allowing distortion away from an ideal square-based pyramidal geometry, thus alleviating steric clash. In both complexes, the *tert*-butyl imido Nb–N bond length (1.756(2) Å in **1**, 1.785(2) Å in **2**) and angle (179.0(2)° in **1**, 175.4(2)° in **2**) are consistent with previously reported Nb mono(imido) complexes.[36,48] The bond metrics of the niobatetrazene moieties in **1** and **2** are also in good agreement with previously reported Nb[36] and Zr[34,35] tetrazene complexes, with a double bond between the two distal N atoms (1.288(3) Å in **1**, 1.272(3) Å in **2**) and single bonds between the metal-bound N atoms and the distal N atoms (1.373(3) Å and 1.381(3) Å in **1**, 1.391(3) Å and 1.365(3) Å in **2**).

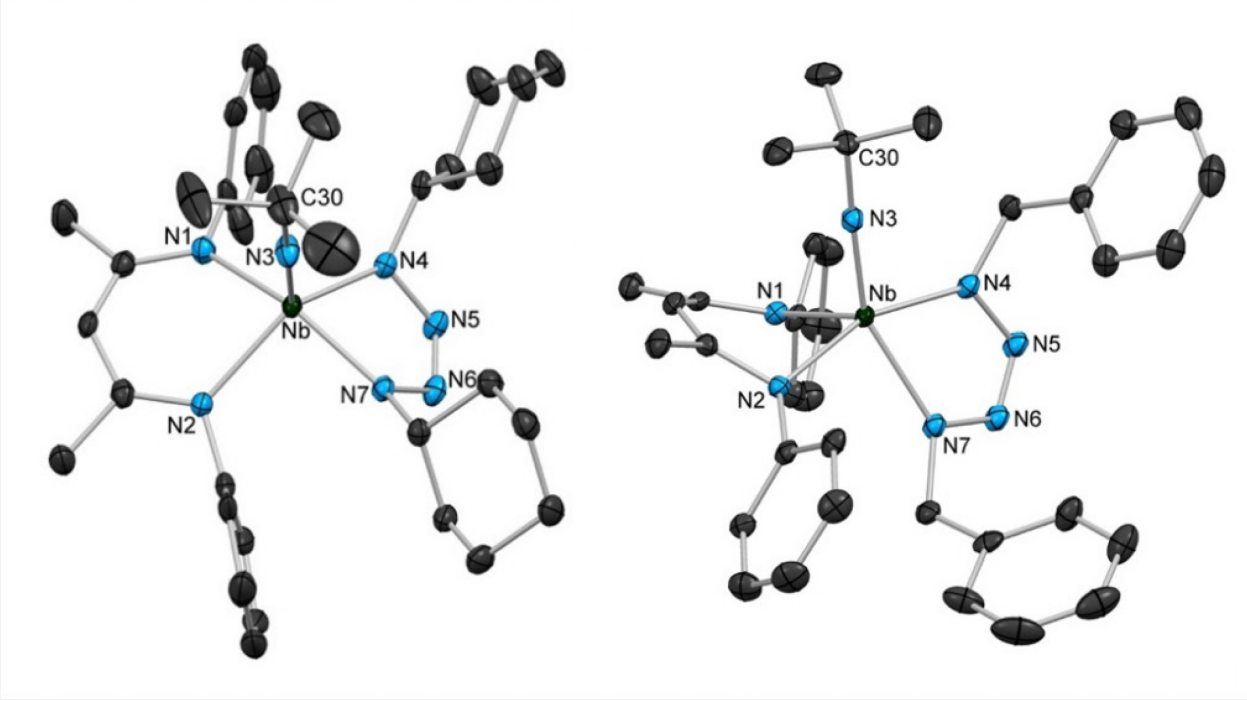


**Figure 1.** Crystal structures of **1** (left) and **2** (right) with 50% probability thermal ellipsoids. H atoms and aryl $^{i}$Pr groups are excluded.

Upon combining **1** with excess $BnN_3$ for 4 h at 60 °C, nearly complete conversion to **2** (and the aforementioned minor side product, again *ca.* 10% relative to **2**), coupled with the loss of cyclohexyl azide, was observed by $^1$H NMR spectroscopy (Figure S7). This reaction likely occurred through a series of reversible [3+2] cycloaddition and cycloreversion steps, proceeding through π-loaded bis(imido) intermediates **A** and **B**, as outlined in Scheme 1. Note that we have previously reported several related Nb(V) bis(imido) complexes supported by bidentate ligands.[30,36,43,45,47] The mixed tetrazene compound (BDI)Nb(N$^t$Bu)(CyNNNNBz) (**3**) was observed as an intermediate that built up during the reaction but disappeared after its completion; this intermediate was most clearly observed when carrying out the solution reaction at room temperature for 16 h (Figures S5-S6). Under similar conditions (vast excess azide and heating to 60 °C), **2** reacted very sluggishly with excess cyclohexyl azide and we did not observe appreciable conversion to **1**, even upon heating overnight, thus indicating that **2** is thermodynamically favored over **1**, likely due to steric considerations, as discussed above.

In an effort to provide evidence for the identity of proposed bis(imido) intermediates **A** and **B** (Scheme 1), we found that addition of one equivalent of *tert*-butyl isocyanide to **1**, with mild heating, resulted in formation of the trapped bis(imido) complex **4a** as yellow crystals in 63% yield (Scheme 2). The $^1$H NMR spectrum of **4a** is consistent with $C_1$ solution symmetry (Figure S8). While the $^1$H and $^{13}$C NMR data suggest that **4a** is quite pure (Figures S8 and S9), combustion analysis was accurate for hydrogen and nitrogen but unsatisfactory for carbon (off by *ca.* 1%); we posit that formation of niobium carbide species could contribute to low carbon content in the combustion analysis. The solid-state structure of **4a** reveals a coordination geometry intermediate between trigonal bipyramidal and square pyramidal ($\tau_5$ = 0.43), with the *tert*-butyl isocyanide group occupying the same plane as the BDI nitrogen atoms and the Nb center (Figure 2 and Table

S3). Both imido groups in bis(imido) complex **4a** are lengthened (*tert*-butyl imido, 1.812(2) Å; cyclohexyl imido, 1.800(2) Å) and bent (*tert*-butyl imido, 159.8(2)°; cyclohexyl imido, 162.5(2)°) relative to mono(imido) complexes **1** and **2**. These are among the longest distances reported for terminal Nb imido bonds; such metrics are observed exclusively in π-loaded bis(imido) complexes.[36,47,48,56] The analogous complex **4b** was cleanly generated in solution upon addition of one equivalent of cyclohexyl isocyanide, as evidenced by $^{1}$H NMR spectroscopy (Scheme 2 and Figure S10).

**Scheme 2.** Syntheses of bis(imido) compounds **4a** and **4b**.

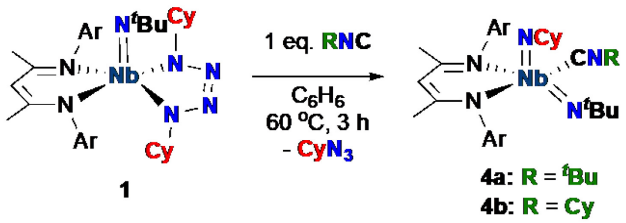


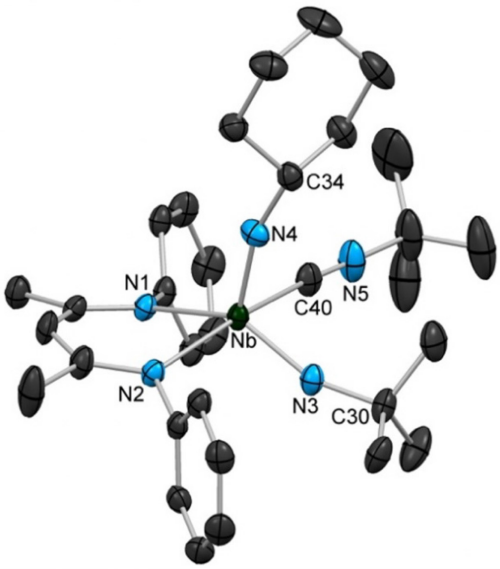

**Figure 2.** Crystal structure of **4a** with 50% probability thermal ellipsoids. H atoms and aryl $^{i}$Pr groups are excluded.

*Computational Studies.*

To gain insight into the mechanism of the transformation outlined in Scheme 1, we turned to computational studies. We carried out our investigation using two methods: the GFN2-xTB variant of Density Functional Tight Binding, a fast semi-empirical quantum chemistry method that is implemented in the xTB software package,[51] and DFT, a well-established computational tool. GFN2-xTB, hereafter referred to as xTB, is parameterized for most atoms in the periodic table and has been shown to produce accurate results for a variety of chemical species, including large transition metal complexes, often with structures similar to those obtained using DFT.[57,58] One of the advantages of the xTB method is a significant reduction in computational time due to the simplified structure of the orbitals along with semiempirical parameterizations for the interactions between them; as such, the xTB method is advantageous for multi-step reactions involving transition metal complexes with complex ligand environments. We sought to determine whether the xTB method could be used to accurately calculate structures and reaction paths for the organometallic sequence discussed above, as compared to DFT.

For computational efficiency, the 2,6-diisopropylphenyl groups of the BDI ligand were truncated to phenyl groups; truncated compounds are denoted by an asterisk (**1***, **2***, **3***, **A***, and **B***). First, compounds **1***, **2***, **3***, **A***, and **B***, as well as benzyl- and cyclohexyl azide, were optimized in the gas phase with xTB (Table S9, refer to the SI for full computational details). We then performed DFT single-point energy calculations on these xTB-optimized structures in order to obtain DFT-corrected xTB free energy values that could be compared to fully DFT-generated

free energy values; these structures are denoted as DFT(xTB) to indicate this mixed approach (Table S9). The xTB-optimized structures were also fully re-optimized using DFT in the gas phase, so we could compare the energies obtained using the two methods (Table S9). We note that use of xTB-optimized structures as a starting point for DFT optimizations resulted in dramatically reduced computational times to DFT convergence. The bond metrics and coordination geometries observed in DFT and xTB-optimized structures **1*** and **2*** are in good agreement between both computational methods and with those found in solid state structures **1** and **2** (Tables S4-S5). The bond metrics and coordination geometries observed in DFT and xTB-optimized structures **3***, **A***, and **B*** are also in good agreement between the two methods (Tables S6-S8).

The HOMO of DFT-optimized **1*** and the LUMO of DFT-optimized **A*** are depicted in Figure 3; corresponding frontier molecular orbital depictions for **2***, **3*** and **B*** can be found in the SI (Figures S11-S13). The HOMO of each tetrazene complex **1***, **2***, and **3*** is primarily composed of the filled π system of the niobatetrazene fragment. The LUMO of each bis(imido) complex **A*** and **B*** is primarily composed of the π* orbitals of the metal center and the two imido groups (*tert*-butyl and cyclohexyl for **A***, *tert*-butyl and benzyl for **B***). The lobes of the π* orbitals where reactivity is observed (cyclohexyl or benzyl) are larger than the π* orbitals of the metal center and the *tert*-butyl imido groups. These frontier molecular orbital depictions are consistent with the observed reactivity patterns.

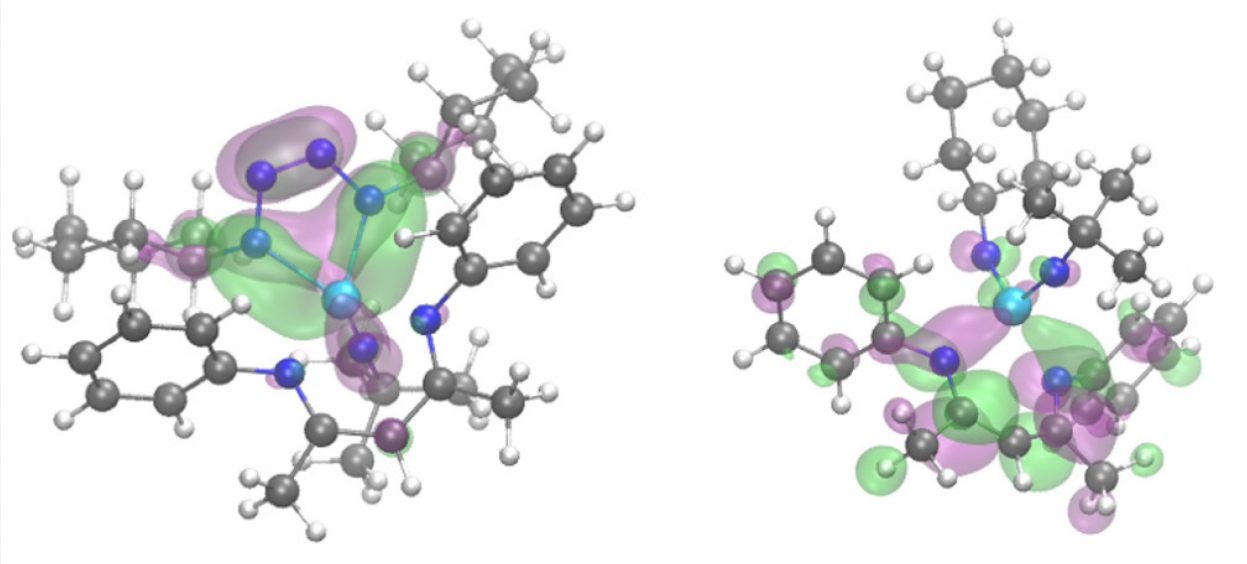

**Figure 3.** Calculated molecular orbital surfaces of DFT-optimized structures: HOMO of **1*** (left) and LUMO of **A*** (right) with an isovalue of 0.03. Color scheme: Nb = cyan, N = blue, C = grey, H = white.

The relative energies of the DFT- and DFT(xTB)-optimized structures are in good agreement with our experimental observations; our findings are summarized in Table 1 and in the reaction coordinate diagram depicted in Figure 4. Comparison of calculated free energies for **1*** and **2*** revealed that **2*** (+ 2 $CyN_3$) is predicted to be slightly more stable than **1*** (+ 2 $BnN_3$) by 3.1 kcal/mol (DFT) and 2.6 kcal/mol (DTF(xTB)); these computational findings are consistent with our experimental observations that **1** can be cleanly converted to **2** upon heating with excess benzyl azide, but **2** cannot be cleanly converted to **1**, even upon heating with excess cyclohexyl azide for extended periods. DFT optimizations estimated the relative free energy of intermediate **3*** to be between that of **1*** and **2***, with **3*** (+ 1 $BnN_3$ + 1 $CyN_3$) more stable than starting material **1*** (+ 2 $BnN_3$) by 1.3 kcal/mol, and less stable than final product **2*** (+ 2 $CyN_3$) by 1.8 kcal/mol. However, using DFT(xTB), we found **3*** (+ 1 $BnN_3$ + 1 $CyN_3$) is calculated to be more stable than

**1*** (+ 2 $BnN_3$) by 3.5 kcal/mol and more stable than **2*** (+ 2 $CyN_3$) by 0.6 kcal/mol. This small difference in relative energies is within typical error bounds for DFT calculations.

**Table 1.** Free energies of sets of isomers relative to **1*** (+ 2 $BnN_3$), calculated using DFT and xTB methods, and the differences between these energies.

| Structure | DFT Relative Free Energy (kcal/mol) | DFT(xTB) Relative Free Energy (kcal/mol) | Δ Relative Free Energy (kcal/mol) |
|---|---|---|---|
| **1*** (+ 2 $BnN_3$) | 0.0 | 0.0 | 0.0 |
| **2*** (+ 2 $CyN_3$) | -3.1 | -2.6 | -0.2 |
| **3*** (+ $BnN_3$ + $CyN_3$) | -1.3 | -3.5 | 2.3 |
| **A*** (+ $CyN_3$ + 2 $BnN_3$) | 23.9 | 23.6 | 0.2 |
| **B*** (+ 2 $CyN_3$ + $BnN_3$) | 23.7 | 24.0 | -0.3 |
| **TS 1* – A*** (+ 2 $BnN_3$) | 45.7 | 44.8 | 0.9 |
| **TS 2* – B***(+ 2 $CyN_3$) | 29.6 | 32.8 | -3.2 |
| **TS 3* – A*** (+ $BnN_3$ + $CyN_3$) | 46.1 | 41.8 | 4.3 |
| **TS 3* – B*** (+ $BnN_3$ + $CyN_3$) | 37.2 | 38.2 | -1.0 |

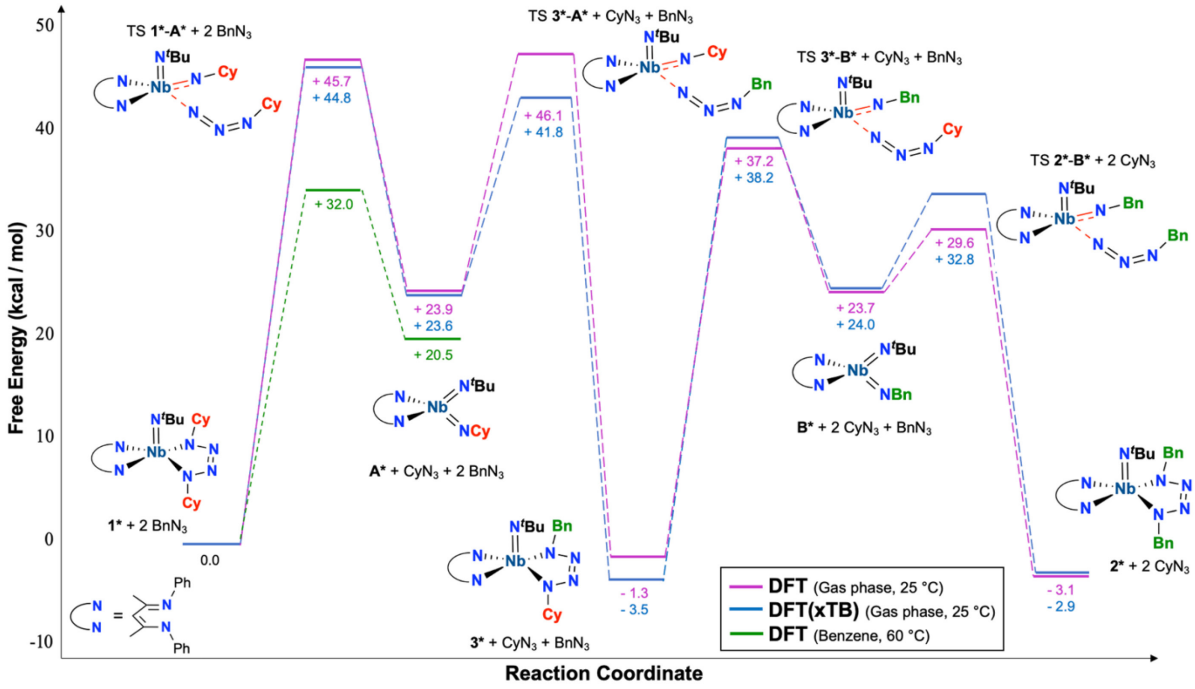


**Figure 4.** DFT (pink) and DFT(xTB) (blue) calculated free energy pathways for the conversion of **1*** (+ 2 $BnN_3$) to **2*** (+ 2 $CyN_3$), in the gas phase at room temperature. DFT (green) calculated free energy pathway for the conversion of **1*** (+ 2 $BnN_3$) to **A*** (+ 2 $BnN_3$ + $CyN_3$), in benzene solvent at 60 °C. Note that all horizontal lines represent isomeric sets of Nb compounds and 2-3 equivalents of the appropriate azides.

We were also able to optimize **A*** and **B*** using both computational methods and found that these structures did not have imaginary frequencies, suggesting that these compounds are indeed true intermediates along this multistep reaction pathway. Using DFT, the relative energies of **A*** (+ 1 $CyN_3$ + 2 $BnN_3$) and **B*** (+ 2 $CyN_3$ + 1 $BnN_3$) are predicted to be 23.9 and 23.7 kcal/mol higher in energy than starting complex **1*** (+ 2 $BnN_3$), respectively. Similarly, using DFT(xTB), we found that **A*** (+ 1 $CyN_3$ + 2 $BnN_3$) is estimated to be 23.6 kcal/mol higher in energy than **1*** (+ 2 $BnN_3$), and **B*** (+ 2 $CyN_3$ + 1 $BnN_3$) is calculated to be 24.0 kcal/mol higher in energy than

**1*** (+ 2 $BnN_3$). Overall, the relative free energies of all reactants, products, and intermediates obtained using DFT(xTB) and DFT methods were quite similar, differing by a maximum of 2.3 kcal/mol (for **3*** + 1 $BnN_3$ + 1 $CyN_3$), thus supporting our decision to use xTB as a faster, yet accurate proxy for DFT. Moreover, the agreement between experiment and theory provides support for our theoretical computational work.

We next set out to find the transition state (TS) structures for this multistep transformation. We again decided to start with xTB methods for this process, in favor of shorter time to convergence. The xTB-optimized TS structures were then used as the initial guesses for DFT TS calculations (refer to the SI for full computational details). The resulting free energies are presented in Figure 4 and Table 1. In general, the magnitudes of the calculated barriers are fairly large, ranging from 29.6 to 46.1 kcal/mol, relative to **1*** (+ 2 $BnN_3$). Values obtained using both methods are quite similar: the greatest difference in relative energy between DFT- and DFT(xTB)-optimized TS structures is 4.3 kcal/mol (TS **3***-**A*** + 1 $BnN_3$ + 1 $CyN_3$).

Although the reactions under study do require relatively forcing conditions (vast excess azide, long reaction times, and heat) to proceed to completion, the computed activation barriers are larger in magnitude than we expected. Assuming the calculations are reasonably accurate, the high activation barriers between tetrazene complexes **1***, **2***, and **3*** and bis(imido) intermediates **A*** and **B*** can be attributed to three sources: ligand truncation, solvation, and temperature. First, truncating ligand 2,6-diisopropylphenyl groups to phenyl groups results in less steric clashing between the bulky substituent groups of the imidos, tetrazene moieties, and BDI ligand. Steric clashing is expected to be more pronounced for tetrazene complexes than bis(imido) complexes, because the tetrazene substituent groups in five-coordinate complexes **1**, **2**, and **3** are forced into closer contact with the ligand substituent groups, while four-coordinate bis(imido) complexes are

relatively less crowded. Thus, we expect that incorporation of full 2,6-diisopropylphenyl ligand groups would lead to a larger degree of destabilization for tetrazene complexes, and smaller destabilizations for transition state and bis(imido) structures. The combination of these destabilizing effects would likely result in lower activation barriers.

In addition to sterics, solvation and temperature also play a role in determining the magnitude of activation barriers; in our original calculations, we neglected to include solvation, and we used standard temperature, which differs from the optimal experimental conditions. To this end, we reoptimized the original DFT-optimized structures of **1***, TS **1***-**A***, **A***, and benzyl- and cyclohexyl azide; benzene solvent was incorporated in the optimization *via* implicit solvation, and a temperature of 60 °C was used for free energy corrections (see SI for full details). These corrections resulted in a 13.7 kcal/mol reduction in the activation barrier between **1 *** (+ 2 $BnN_3$) and TS **1*-A*** (+ 2 $BnN_3$)**,** from 45.7 (DFT) to 32.0 kcal/mol, and lowered the relative energy of **A*** (+ 2 $BnN_3$ + 1 $CyN_3$) by 3.4 kcal/mol (Figure 4 and Table S10). Thus, it can be inferred that temperature and solvation do indeed play a large role in determining magnitude of activation energy barriers along this reaction pathway.

Finally, reaction path calculations (either conventional Intrinsic Reaction Coordinate calculations or fixed-step-length gradient descent calculations; see SI for full details) carried out using the xTB method confirmed that the transition state structures TS **1***-**A***, TS **3***-**A***, TS **3***-**B***, and TS **2***-**B*** connect in single steps to the optimized structures of **1***, **3***, **3***, and **2***, respectively (Figure 5 and Figure S14). Notably, the computational savings gained through use of the xTB method over DFT is even greater for these reaction path calculations than for the aforementioned geometry optimizations and TS calculations. During the retrocycloaddition transformation of a niobatetrazene complex to a bis(imido) complex (i.e., from **1*** to **A*** and from

**3*** to **B***), we expected the two bonds being broken, Nb–N1 and N3–N4 (Figure 5a inset), to break nearly simultaneously, resulting in the formation of a leaving azide group and a Nb-imido moiety. However, the reaction path results suggest that the transformation is far from synchronously concerted: first, the Nb–N1 bond breaks, then a *new* bond forms between Nb and N3 (the terminal N atom of the leaving azide group), forming a three-membered Nb–N3–N4 ring. Subsequently, the N3–N4 bond of the three-membered ring breaks, forming a complex bearing a terminally-bound azide group and an imido moiety; we recently reported a similar Nb(V) bis(imido)-azide complex.[36] The Nb–azide bond continues to lengthen, ultimately yielding the predicted TS structure. We observe similar results for the forward-sense [3+2] cycloaddition transformations: reaction path scans from TS **3*-A*** to **3*** (Figure 5b) and TS **2*-B*** to **2*** (Figure S14b) also show construction of a new Nb–N3 bond punctuating Nb–N1 and N3–N4 bond formation events.

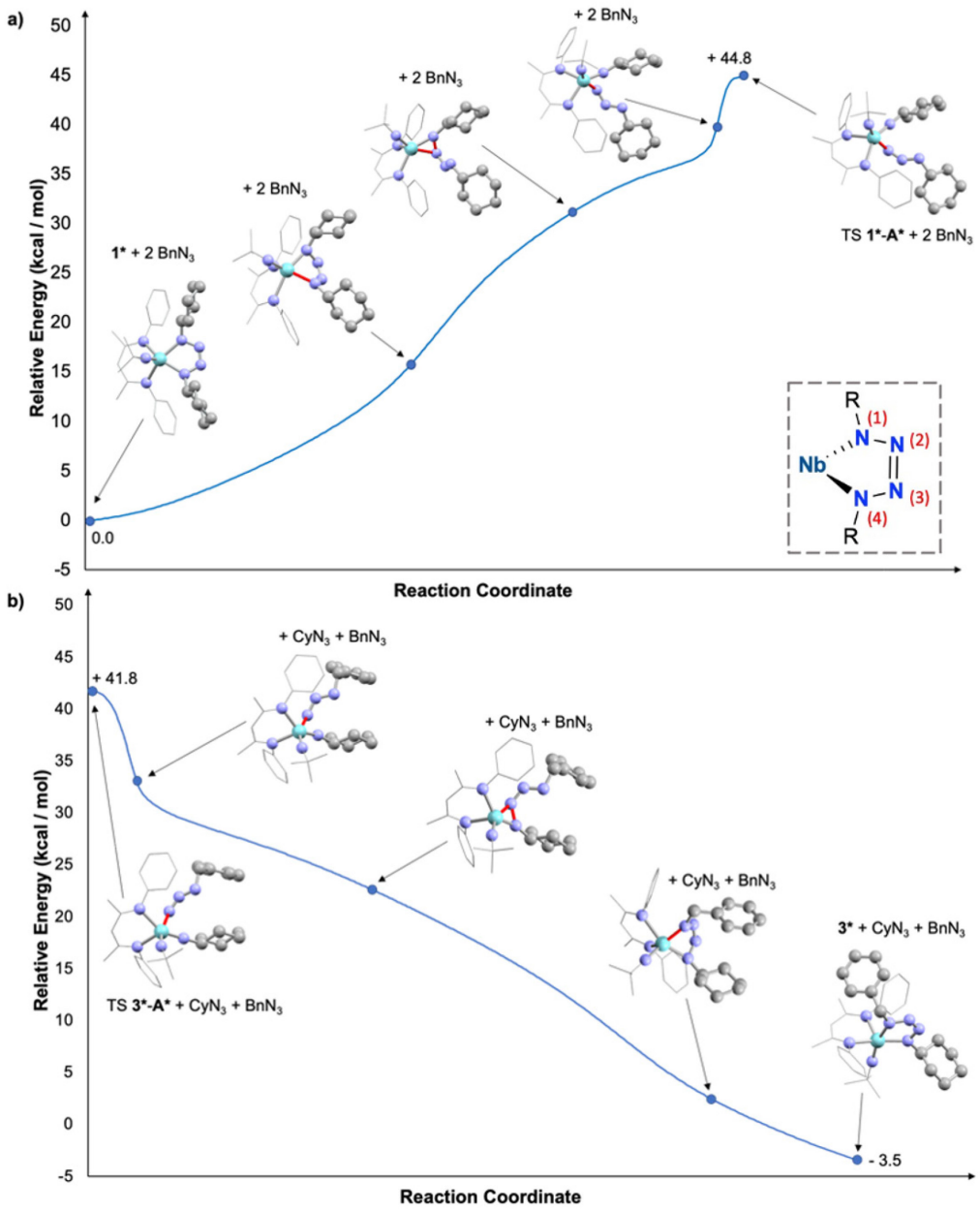


**Figure 5.** Reaction path diagrams for the transformation from a) **1*** to TS **1*-A*** and b) TS **3*-A*** to **3***. The inset in a) depicts a numbered representation of the nitrogen atoms in niobatetrazene complexes **1***, **2***, and **3***; R = Cy, Bn.

Overall, the individual cycloaddition and retrocycloaddition processes in this reaction pathway are predicted to occur *via* an asynchronous concerted reaction mechanism: Nb–N1 and N3–N4 bond cleavage/formation occur at distinct points along the reaction coordinate and are separated by the formation of a Nb–N3 bond, while no stable intermediates are formed along the reaction path. The asynchronous nature of this reaction pathway is made apparent by the appearance of a 'shoulder' in each of the reaction path diagrams.[33,59-61] While others have reported computational studies of asynchronous[59,60] and even "highly asynchronous" cycloadditions,[61] we could find no other reports of bond formation disrupting the two bond formation/cleavage events.

## Conclusion

A BDI-supported Nb imido system was shown to be capable of mediating azide metathesis *via* a series of [3+2] and retro-[3+2] cycloadditions, passing through π-loaded bis(imido) intermediates as evidenced by NMR spectroscopic, crystallographic, and computational studies. We found benzyl tetrazene complex **2** to be more thermodynamically stable than cyclohexyl tetrazene complex **1** *via* both experimental and computational studies, likely due to steric considerations. In our computational investigations, we obtained very similar optimization results using two methods, xTB and DFT, thus highlighting the validity and applicability of the xTB software package for studying systems involving large transition metal complexes. We also note that use of xTB-optimized structures as a starting point for DFT optimizations results in dramatically reduced computational times to DFT convergence and thus provides a useful method for those studying very large and/or complex molecules. Reaction path calculations for this multistep transformation suggested that each individual cycloaddition or retrocycloaddition process occurs *via* an asynchronous concerted mechanism and predicted the formation of a temporary niobaazacyclopropane moiety which, however, was not calculated to be a minimum on

the free energy surface. Future work will focus on expanding experimental and computational studies of this system toward [3+2] cycloadditions of 1,3-dipoles other than organic azides, such as diazo and nitro substrates.

## Experimental

*General Considerations.* Unless otherwise stated, all reactions were performed under an atmosphere of dry $N_2$ using standard Schlenk line techniques or in an MBraun inert atmosphere glovebox under an atmosphere of nitrogen (<1.0 ppm $O_2/H_2O$). All glassware, cannulae, and Celite were stored in an oven at *ca.* 150 °C for at least 12 h prior to use. Molecular sieves (4 Å) were activated by heating to 200 °C overnight under vacuum and then stored in a glovebox. NMR spectra were obtained at ambient temperature, unless otherwise noted, using Bruker AVB-400, AV-500, DRX-500, and AV-600 spectrometers. $^1$H and $^{13}$C{$^1$H} NMR chemical shifts (δ) were reported relative to residual solvent peaks. $^1$H and $^{13}$C NMR assignments were routinely confirmed by $^1$H-$^1$H (COSY and NOESY) and $^1$H-$^{13}$C (HSQC and HMBC) experiments. Melting points were determined using an Optimelt SRS automated melting point system using sealed capillaries prepared under an atmosphere of dry $N_2$. Elemental analyses were determined either at the College of Chemistry, University of California, Berkeley, or at the School of Human Sciences, Science Center, London Metropolitan University. X-ray structural determinations were performed at CHEXRAY, University of California, Berkeley, on SMART APEX I and SMART APEX II QUAZAR diffractometers.

*Materials.* Benzene and *n*-hexane were dried and degassed using a Phoenix solvent drying system commercially available from JC Meyer Solvent Systems. Hexamethyldisiloxane (HMDSO) was vacuum distilled from sodium/benzophenone, degassed by sparging with nitrogen,

and stored over molecular sieves. $C_6D_6$ was dried using sodium/benzophenone, degassed with three freeze-pump-thaw cycles, and vacuum-transferred prior to storage in a glovebox over molecular sieves. *Tert*-butyl isocyanide was degassed with three freeze-pump-thaw cycles and stored over molecular sieves. (BDI)Nb(N$^t$Bu)($\eta^6$-$C_6H_6$)[62] (BDI = ArNC(Me)CHC(Me)NAr, Ar = 2,6-diisopropylphenyl) was prepared according to the literature procedure. All other reagents, including cyclohexyl azide, benzyl azide, and cyclohexyl isocyanide, were acquired from commercial sources and used as received.

*Warning!* Organic azides ($RN_3$) are potentially explosive substances that should be handled with extreme care.

*Synthetic Procedures.*

**(BDI)Nb(N$^t$Bu)(CyNNNNCy) (1).** (BDI)Nb(N$^t$Bu)($\eta^6$-$C_6H_6$) (300 mg, 0.450 mmol) was added to a 20 mL vial. In a separate vial, cyclohexyl azide (120 mg, 0.960 mmol) was dissolved in 5 mL of hexane. The cyclohexyl azide solution was added to the (BDI)Nb(N$^t$Bu)($\eta^6$-$C_6H_6$), and the mixture was stirred until all (BDI)Nb(N$^t$Bu)($\eta^6$-$C_6H_6$) had dissolved. Upon addition of the azide solution, visible effervescence of dinitrogen was observed, which subsided within 5 min. The vial was capped and left at room temperature for an additional 3 h, resulting in a gradual lightening of the color from dark red to red and precipitation of red crystalline material. The vial was stored at -40 ˚C overnight, resulting in further precipitation of crystalline material. The crystals were isolated by removal of the supernatant, and residual solvent was removed under vacuum. Yield: 280 mg, 77%. $^1$H NMR (500 MHz, 293 K, $C_6D_6$): δ = 7.18–7.10 (m, 6H, Ar), 5.06 (s, 1H, *H*C(C(Me)NAr)$_2$), 3.77 (sep, 2H, C*H*Me$_2$), 3.14 (m, 2H, Cy C*H*), 2.62 (sep, 2H, C*H*Me$_2$), 1.71-1.60 (m, 8H, Cy C$H_2$), 1.56–1.36 (m, 3H, Cy C$H_2$), 1.52 (d, 6H, CH*Me*$_2$), 1.48 (s, 6H, HC(C(*Me*)NAr)$_2$), 1.46 (s, 9H, $^t$Bu), 1.40 (d, 6H, CH*Me*$_2$), 1.33-0.94 (m, 9H, Cy C$H_2$), 1.27 (d,

6H, CH*Me*$_2$), 1.01 (d, 6H, CH*Me*$_2$). $^{13}$C NMR (150 MHz, 293 K, $C_6D_6$): δ = 169.5 (HC(*C*(Me)NAr)$_2$), 150.9 (Ar), 143.0 (Ar), 141.0 (Ar), 126.5 (Ar), 125.3 (Ar), 124.0 (Ar), 101.3 (H*C*(C(Me)NAr)$_2$), 71.3 ($C_\alpha$, $^t$Bu), 64.9 (*C*H, Cy), 33.8 ($C_\beta$, $^t$Bu), 33.6 (*C*H$_2$, Cy), 29.3 (*C*HMe$_2$), 28.3 (*C*HMe$_2$), 27.2 (*C*H$_2$, Cy), 26.8 (HC(C(*Me*)NAr)$_2$), 26.4 (*C*H$_2$, Cy), 25.4 (CH*Me*$_2$), 25.3 (CH*Me*$_2$), 25.3 (CH*Me*$_2$), 24.6 (CH*Me*$_2$). Anal. calcd (%) for $Nb_1N_7C_{45}H_{72}$: C, 67.22; H, 9.03; N, 12.19. Found: C, 67.01; H, 9.17; N, 12.08. MP: 146–150 ˚C.

**(BDI)Nb(N$^t$Bu)(BnNNNNBn) (2).** (BDI)Nb(N$^t$Bu)(η$^6$-$C_6H_6$) (500 mg, 0.760 mmol) was dissolved in 5 mL of benzene in a 20 mL vial. In a separate vial, benzyl azide (200 mg, 1.50 mmol) was dissolved in 5 mL of hexane. The benzyl azide solution was added to the solution of (BDI)Nb(N$^t$Bu)(η$^6$-$C_6H_6$), and the mixture was stirred until all (BDI)Nb(N$^t$Bu)(η$^6$-$C_6H_6$) had dissolved. Upon addition of the azide solution, visible effervescence of dinitrogen was observed, which within 5 min. The resulting solution was stirred at 60 °C for 3 h under an $N_2$ atmosphere, resulting in a gradual lightening of the color from dark red to red. The volatile materials were removed under vacuum, leaving a dark red oily residue. The residue was extracted with hexane (3 × 2 mL); upon dissolution of the residue in hexane, red crystalline material immediately began to form. The crystalline material was isolated by removal of the supernatant and residual solvent was removed under vacuum. The supernatant was concentrated and stored at -40 ˚C overnight, yielding an additional crop of red crystals that were isolated and dried under vacuum. Yield: 220 mg, 35% over two crops. A minor (*ca.* 10% relative to **2**) reaction product was observed by $^1$H NMR spectroscopy; we posit this species is the product of cycloaddition across the *tert*-butyl imido group, (BDI)Nb(NBn)($^t$BuNNNNBn)). $^1$H NMR (400 MHz, 293 K, $C_6D_6$): δ = 7.22–6.97 (m, 16H, Ar/Bn), 5.17 (s, 1H, *H*C(C(Me)NAr)$_2$), 4.22 (s, 4H, C*H*$_2$Ph), 3.70 (sep, 2H, C*H*Me$_2$), 2.67 (sep, 2H, C*H*Me$_2$), 1.62 (s, 6H, HC(C(*Me*)NAr)$_2$), 1.51 (d, 6H, CH*Me*$_2$), 1.31 (d, 6H, CH*Me*$_2$), 1.29 (s,

9H, $^t$Bu), 1.25 (d, 6H, CH*Me*$_2$), 0.99 (d, 6H, CH*Me*$_2$). $^{13}$C NMR (150 MHz, 293 K, $C_6D_6$): δ = 169.7 (HC(*C*(Me)NAr)$_2$), 149.3 (Ar or Bn), 143.1 (Ar or Bn), 142.3 (Ar or Bn), 142.1 (Ar or Bn), 128.1 (Ar or Bn), 127.9 (Ar or Bn), 127.0 (Ar or Bn), 126.3 (Ar or Bn), 124.9 (Ar or Bn), 124.1 (Ar or Bn), 102.0 (H*C*(C(Me)NAr)$_2$), 71.7 (C$_\alpha$, $^t$Bu), 58.7 (*C*H$_2$Ph), 33.4 (C$_\beta$, $^t$Bu), 29.7 (*C*HMe$_2$), 28.0 (*C*HMe$_2$), 26.7 (HC(C(*Me*)NAr)$_2$), 26.3 (CH*Me*$_2$), 25.6 (CH*Me*$_2$), 24.9 (CH*Me*$_2$), 24.3 (CH*Me*$_2$). Anal. calcd (%) for $Nb_1N_7C_{47}H_{64}$: C, 68.85; H, 7.87; N, 11.96. Found: C, 68.73; H, 7.94; N, 11.77. MP: 137–142 ˚C.

**Solution generation of (BDI)Nb(N$^t$Bu)(BnNNNNBn) (2) from (BDI)Nb(N$^t$Bu)(CyNNNNCy) (1).** Solid **1** (20.0 mg, 0.028 mmol) was combined with 10 eq. benzyl azide, dissolved in $C_6D_6$, and transferred to a J. Young NMR tube. The tube was sealed and heated to 60 $^o$C for 4 h, resulting in nearly complete conversion to **2** and $CyN_3$. The $^1$H NMR spectrum of **2** generated *via* this route exactly matched that of isolated **2** (including the presence of a minor side product, *ca.* 10% relative to **2**).

**Observation of (BDI)Nb(N$^t$Bu)(BnNNNNCy) (3) by $^1$H NMR Spectroscopy.** Compound **3** was observed as an intermediate by $^1$H NMR spectroscopy upon allowing **1** (20.0 mg, 0.028 mmol) to react with 10 eq. benzyl azide at room temperature for 16 h. $^1$H NMR (600 MHz, 293 K, $C_6D_6$): δ = 7.32–6.92 (m, 11H, Ar), 5.13 (s, 1H, *H*C(C(Me)NAr)$_2$), 4.07 (s, 2H, Bn C*H*$_2$), 3.71 (sep, 2H, C*H*Me$_2$), 3.34 (m, 1H, Cy C*H*), 2.66 (sep, 2H, C*H*Me$_2$), 1.69–0.98 (m, 10H, Cy C*H*$_2$), 1.56 (s, 6H, HC(C(*Me*)NAr)$_2$), 1.43 (d, 6H, CH*Me*$_2$), 1.38 (s, 9H, $^t$Bu), 1.36 (d, 6H, CH*Me*$_2$), 1.25 (d, 6H, CH*Me*$_2$), 0.99 (d, 6H, CH*Me*$_2$).

**(BDI)Nb(N$^t$Bu)(NCy)(CN$^t$Bu) (4a).** Compound **1** (300 mg, 0.370 mmol) was added to a 50 mL flask and dissolved in 5 mL of benzene to give a red solution. *Tert*-butyl isocyanide (84.0 μL, 62.0 mg, 0.750 mmol) was added by a micro-syringe. The flask was sealed, and the solution was heated

at 60 °C for 3 h, resulting in a color change from red to orange. The volatile materials were removed under vacuum, leaving an orange residue. The residue was extracted with HMDSO (3 × 2 mL), and the combined extracts were concentrated under vacuum to a final volume of *ca.* 2 mL. The solution was stored at -40 ˚C overnight, yielding yellow crystals of **4a**. The crystals were isolated by removal of the supernatant, and residual solvent was removed under vacuum. Yield: 180 mg, 63% over three crops. $^{1}$H NMR (600 MHz, 293 K, $C_6D_6$): δ = 7.26–7.16 (m, 3H, Ar), 7.06–6.98 (m, 3H, Ar), 5.04 (s, 1H, *H*C(C(Me)NAr)$_2$), 4.48 (m, 1H, Cy C*H*), 4.12 (sep, 1H, C*H*Me$_2$), 3.76 (sep, 1H, C*H*Me$_2$), 3.56 (sep, 1H, C*H*Me$_2$), 3.51 (sep, 1H, C*H*Me$_2$), 2.44 (br d, 1H, Cy), 2.07 (br d, 1H, Cy), 1.85–1.15 (m, 8H, Cy), 1.74 (d, 3H, CH*Me*$_2$), 1.71 (s, 3H, HC(C(*Me*)NAr)$_2$), 1.65 (s, 3H, HC(C(*Me*)NAr)$_2$), 1.61 (d, 3H, CH*Me*$_2$), 1.46 (d, 3H, CH*Me*$_2$), 1.40 (d, 3H, CH*Me*$_2$), 1.37 (d, 3H, CH*Me*$_2$), 1.35 (d, 3H, CH*Me*$_2$), 1.29 (d, 3H, CH*Me*$_2$), 1.21 (d, 3H, CH*Me*$_2$), 1.09 (s, 9H, NbN$^t$Bu), 0.78 (s, 9H, C≡N$^t$Bu). $^{13}$C NMR (150 MHz, 293 K, $C_6D_6$): δ = 166.1 (HC(*C*(Me)NAr)$_2$), 165.7 (HC(*C*(Me)NAr)$_2$), 152.5 (Ar), 152.0 (Ar), 143.0 (Ar), 142.3 (Ar), 142.2 (Ar), 142.2 (Ar), 125.3 (Ar), 125.1 (Ar), 124.4 (Ar), 124.4 (Ar), 124.3 (Ar), 123.4 (Ar), 99.3 (H*C*(C(Me)NAr)$_2$), 71.3 (*C*H, Cy), 64.7 ($C_\alpha$, NbN$^t$Bu), 56.0 ($C_\alpha$, C≡N$^t$Bu), 38.6 (Cy), 38.4 (Cy), 33.2 ($C_\beta$, NbN$^t$Bu), 29.4 ($C_\beta$, C≡N$^t$Bu), 28.7 (*C*HMe$_2$), 28.6 (*C*HMe$_2$), 28.0 (*C*HMe$_2$), 27.7 (*C*HMe$_2$), 27.0 (Cy), 26.9 (Cy), 26.7 (CH*Me*$_2$), 26.1 (Cy), 25.9 (CH*Me*$_2$), 25.3 (HC(C(*Me*)NAr)$_2$), 25.2 (CH*Me*$_2$), 25.1 (CH*Me*$_2$), 24.9 (HC(C(*Me*)NAr)$_2$), 24.9 (CH*Me*$_2$), 24.8 (CH*Me*$_2$), 24.4 (CH*Me*$_2$), 23.8 (CH*Me*$_2$). A resonance corresponding to the Nb-coordinated isocyanide C atom (*C*≡N$^t$Bu) was not observed in the $^{13}$C NMR spectrum. Anal. calcd (%) for $Nb_1N_5C_{47}H_{70}\cdot 0.5C_6H_{18}OSi_2$: C, 68.31; H, 9.06; N, 7.97. Found: C, 67.40; H, 9.18; N, 8.23. MP: 136 ˚C (dec).

**Observation of (BDI)Nb(N$^t$Bu)(NCy)(CNCy) (4b) by $^1$H NMR Spectroscopy.** Compound **1** (10.0 mg, 0.012 mmol) and cyclohexyl isocyanide (2.70 mg, 0.025 mmol) were combined in a 4 mL vial and the solid mixture was dissolved in $C_6D_6$ (0.400 mL). The resulting solution was transferred to a J. Young NMR tube. The solution was heated at 60 ˚C for 3 h, resulting in a color change from red to orange. A $^1$H NMR spectrum indicated clean conversion to **4b** and dicyclohexyl carbodiimide. $^1$H NMR (400 MHz, 293 K, $C_6D_6$): δ = 7.29–7.16 (m, 3H, Ar), 7.10–6.96 (m, 3H, Ar), 5.06 (s, 1H, *H*C(C(Me)NAr)$_2$), 4.48 (m, 1H, NbNCy C*H*), 4.13 (sep, 1H, C*H*Me$_2$), 3.81 (sep, 1H, C*H*Me$_2$), 3.58 (sep, 1H, C*H*Me$_2$), 3.53 (sep, 1H, C*H*Me$_2$), 2.88 (m, 1H, CNCy C*H*), 2.48 (br d, 1H, Cy), 2.09 (br d, 1H, Cy), 1.90–0.67 (m, 20H, Cy), 1.75 (d, 3H, CH*Me*$_2$), 1.72 (s, 3H, HC(C(*Me*)NAr)$_2$), 1.68 (s, 3H, HC(C(*Me*)NAr)$_2$), 1.62 (d, 3H, CH*Me*$_2$), 1.50 (d, 3H, CH*Me*$_2$), 1.41 (d, 6H, CH*Me*$_2$), 1.36 (d, 3H, CH*Me*$_2$), 1.30 (d, 3H, CH*Me*$_2$), 1.23 (d, 3H, CH*Me*$_2$), 1.12 (s, 9H, $^t$Bu).

## ASSOCIATED CONTENT

**Supporting Information**. NMR spectra, crystallographic information, and computational details.

**Accession Codes.** CCDC 2120976–2120978 contain the supplementary crystallographic data for this paper. These data can be obtained free of charge *via* www.ccdc.cam.ac.uk/data_request/cif, or by emailing data_request@ccdc.cam.ac.uk, or by contacting The Cambridge Crystallographic Data Centre, 12 Union Road, Cambridge CB2 1EZ, UK; fax: +44 1223 336033.

## AUTHOR INFORMATION

**Corresponding Author**

*John Arnold - Department of Chemistry, University of California, Berkeley, California 94720, United States; Email: arnold@berkeley.edu

**Notes**

The authors declare no competing financial interest.

ACKNOWLEDGMENT

We thank the NSF (Grant No. CHE-1465188 and 1954612) for financial support. J.I.F. acknowledges support from an NSF graduate research fellowship (Grant No. DGE 1752814). The UC Berkeley Molecular Graphics and Computation Facility is supported by the NIH (Grant No. S10OD023532). The Advanced Light Source (ALS) is supported by the U.S. DOE (Contract No. DE-AC02-05CH11231). The CHEXRAY X-ray crystallographic facility is supported by the NIH (Grant No. S10-RR027172). We thank E. A. Cortes, E. T. Ouellette, Dr. M. A. Boreen, Dr. T. D. Lohrey, Dr. J. A. Ziegler, Dr. T. Saito, Prof. T. L. Gianetti, and Prof. L. Maron for helpful discussions.

REFERENCES

(1) Nugent, W. A.; Mayer, J. M. *Metal-Ligand Multiple Bonds*; Wiley Interscience, 1988.

(2) Wigley, D. E. Organoimido Complexes of the Transition Metals. In *Progress in Inorganic Chemistry*, Vol. 42; Karlin, K. D., Ed.; John Wiley & Sons, Inc., 1994; pp 239-482.

(3) Webb, J. R.; Burgess, S. A.; Cundari, T. R.; Gunnoe, T. B. Activation of carbon-hydrogen bonds and dihydrogen by 1,2-CH-addition across metal-heteroatom bonds. *Dalton Trans.* **2013**, *42*, 16646-16665.

(4) Kawakita, K.; Parker, B. F.; Kakiuchi, Y.; Tsurugi, H.; Mashima, K.; Arnold, J.; Tonks, I. A. Reactivity of terminal imido complexes of group 4–6 metals: Stoichiometric and catalytic reactions involving cycloaddition with unsaturated organic molecules. *Coord. Chem. Rev.* **2020**, *407*, 213118-213141.

(5) Walsh, P. J.; Hollander, F. J.; Bergman, R. G. Generation, Alkyne Cycloaddition, Arene C-H Activation, N-H Activation, and Dative Ligand Trapping Reactions of the First Monomeric Imidozirconocene ($Cp_2Zr$=NR) Complexes. *J. Am. Chem. Soc.* **1988**, *110*, 8729-8731.

(6) Cummins, C. C.; Baxter, S. M.; Wolczanski, P. T. Methane and Benzene Activation via Transient ($t$-$Bu_3SiNH)_2Zr$=NSi-$t$-$Bu_3$. *J. Am. Chem. Soc.* **1988**, *110*, 8731-8733.

(7) Duncan, A. P.; Bergman, R. G. Selective Transformations of Organic Compounds by Imidozirconocene Complexes. *Chem. Rec.* **2002**, *2*, 431-445.

(8) Chu, J.; Lu, E.; Chen, Y.; Leng, X. Reversible Addition of the Si-H Bond of Phenylsilane to the Sc=N Bond of a Scandium Terminal Imido Complex. *Organometallics* **2013**, *32*, 1137-1140.

(9) Chu, J.; Han, X.; Kefalidis, C. E.; Zhou, J.; Maron, L.; Leng, X.; Chen, Y. Lewis Acid Triggered Reactivity of a Lewis Base Stabilized Scandium-Terminal Imido Complex: C-H Bond Activation, Cycloaddition, and Dehydrofluorination. *J. Am. Chem. Soc.* **2014**, *136*, 10894-10897.

(10) Wolczanski, P. T. Activation of Carbon-Hydrogen Bonds via 1,2-RH-Addition/-Elimination to Early Transition Metal Imides. *Organometallics* **2018**, *37*, 505-516.

(11) Heyduk, A. F.; Zarkesh, R. A.; Nguyen, A. I. Designing Catalysts for Nitrene Transfer Using Early Transition Metals and Redox-Active Ligands. *Inorg. Chem.* **2011**, *50*, 9849-9863.

(12) La Pierre, H. S.; Arnold, J.; Toste, F. D. *Z*-Selective Semihydrogenation of Alkynes Catalyzed by a Cationic Vanadium Bisimido Complex. *Angew. Chem., Int. Ed.* **2011**, *50*, 3900-3903.

(13) Gianetti, T. L.; La Pierre, H. S.; Arnold, J. Group 5 Imides and Bis(Imide)s as Selective Hydrogenation Catalysts. *Eur. J. Inorg. Chem.* **2013**, *2013*, 3771-3783.

(14) Pearce, A. J.; Harkins, R. P.; Reiner, B. R.; Wotal, A. C.; Dunscomb, R. J.; Tonks, I. A. Multicomponent Pyrazole Synthesis from Alkynes, Nitriles, and Titanium Imido Complexes via Oxidatively Induced N-N Bond Coupling. *J. Am. Chem. Soc.* **2020**, *142*, 4390-4399.

(15) Gilbert, Z. W.; Hue, R. J.; Tonks, I. A. Catalytic Formal [2+2+1] Synthesis of Pyrroles from Alkynes and Diazenes via $Ti^{II}/Ti^{IV}$ Redox Catalysis. *Nat. Chem.* **2016**, *8*, 63-68.

(16) Kawakita, K.; Beaumier, E. P.; Kakiuchi, Y.; Tsurugi, H.; Tonks, I. A.; Mashima, K. Bis(Imido)Vanadium(V)-Catalyzed [2+2+1] Coupling of Alkynes and Azobenzenes Giving Multisubstituted Pyrroles. *J. Am. Chem. Soc.* **2019**, *141*, 4194-4198.

(17) Pohlki, F.; Doye, S. The Catalytic Hydroamination of Alkynes. *Chem. Soc. Rev.* **2003**, *32*, 104-114.

(18) Bytschkov, I.; Doye, S. Group-IV Metal Complexes as Hydroamination Catalysts. *Eur. J. Org. Chem.* **2003**, *2003*, 935-946.

(19) Müller, T. E.; Hultzsch, K. C.; Yus, M.; Foubelo, F.; Tada, M. Hydroamination: Direct Addition of Amines to Alkenes and Alkynes. *Chem. Rev.* **2008**, *108*, 3795-3892.

(20) Cao, C.; Shi, Y.; Odom, A. L. A Titanium-Catalyzed Three-Component Coupling to Generate α,β-Unsaturated β-Iminoamines. *J. Am. Chem. Soc.* **2003**, *125*, 2880-2881.

(21) Basuli, F.; Aneetha, H.; Huffman, J. C.; Mindiola, D. J. A Fluorobenzene Adduct of Ti(IV), and Catalytic Carboamination to Prepare α,β-Unsaturated Imines and Triaryl-Substituted Quinolines. *J. Am. Chem. Soc.* **2005**, *127*, 17992-17993.

(22) Davis-Gilbert, Z. W.; Yao, L. J.; Tonks, I. A. Ti-Catalyzed Multicomponent Oxidative Carboamination of Alkynes with Alkenes and Diazenes. *J. Am. Chem. Soc.* **2016**, *138*, 14570-14573.

(23) Ruck, R. T.; Bergman, R. G. Reactions of Imines with Azazirconacyclobutenes and Generation of Electron-Deficient Imidozirconocene Complexes. *Organometallics* **2004**, *23*, 2231-2233.

(24) Ruck, R. T.; Zuckerman, R. L.; Krska, S. W.; Bergman, R. G. Carboamination: Additions of Imine C=N Bonds across Alkynes Catalyzed by Imidozirconium Complexes. *Angew. Chem., Int. Ed.* **2004**, *43*, 5372-5374.

(25) McInnes, J. M.; Mountford, P. Transition Metal Imide/Organic Imine Metathesis Reactions: *Unexpected Observations*. *Chem. Commun.* **1998**, 1669-1670.

(26) Zuckerman, R. L.; Krska, S. W.; Bergman, R. G. Zirconium-Mediated Metathesis of Imines: A Study of the Scope, Longevity, and Mechanism of a Complicated Catalytic System. *J. Am. Chem. Soc.* **2000**, *122*, 751-761.

(27) Meyer, K. E.; Walsh, P. J.; Bergman, R. G. Zirconium-Mediated Imine Metathesis. Synthesis of 2,4-Diaza-1-Zirconiacyclobutanes and the Mechanism of Their Reactions with Imines and Alkynes. *J. Am. Chem. Soc.* **1994**, *116*, 2669-2670.

(28) Bruno, J. W.; Li, X. J. Use of Niobium(III) and Niobium(V) Compounds in Catalytic Imine Metathesis under Mild Conditions. *Organometallics* **2000**, *19*, 4672-4674.

(29) Burland, M. C.; Pontz, T. W.; Meyer, T. Y. Role of Trace Amine in the Metathesis of Imines by $CpTa(=NR)Cl_2$. *Organometallics* **2002**, *21*, 1933-1941.

(30) Obenhuber, A. H.; Gianetti, T. L.; Bergman, R. G.; Arnold, J. Regioselective [2+2] and [4+2] Cycloaddition Reactivity in an Asymmetric Niobium(Bisimido) Moiety towards Unsaturated Organic Molecules. *Chem. Commun.* **2015**, *51*, 1278-1281.

(31) Woodward, R. B.; Hoffmann, R. The Conservation of Orbital Symmetry. *Angew. Chem., Int. Ed.* **1969**, *8*, 781-853.

(32) Huisgen, R. The Concerted Nature of 1,3-Dipolar Cycloadditions and the Question of Diradical Intermediates. *J. Org. Chem.* **1976**, *41*, 403-419.

(33) Houk, K. N.; Gonzalez, J.; Li, Y. Pericyclic Reaction Transition States: Passions and Punctilios, 1935-1995. *Acc. Chem. Res.* **1995**, *28*, 81-90.

(34) Gehrmann, T.; Lloret Fillol, J.; Wadepohl, H.; Gade, L. H. Synthesis, Characterization, and Thermal Rearrangement of Zirconium Tetraazadienyl and Pentaazadienyl Complexes. *Organometallics* **2012**, *31*, 4504-4515.

(35) Meyer, K. E.; Walsh, P. J.; Bergman, R. G. A Mechanistic Study of the Cycloaddition–Cycloreversion Reactions of the Zirconium–Imido Complex $Cp_2Zr(N\text{-}t\text{-}Bu)(THF)$ with Organic Imines and Azides. *J. Am. Chem. Soc.* **1995**, *117*, 974-985.

(36) Obenhuber, A. H.; Gianetti, T. L.; Berrebi, X.; Bergman, R. G.; Arnold, J. Reaction of (Bisimido)Niobium(V) Complexes with Organic Azides: [3 + 2] Cycloaddition and Reversible

Cleavage of β-Diketiminato Ligands Involving Nitrene Transfer. *J. Am. Chem. Soc.* **2014**, *136*, 2994-2997.

(37) Zhou, E.; Ren, W.; Hou, G.; Zi, G.; Fang, D. C.; Walter, M. D. Small Molecule Activation Mediated by a Thorium Terminal Imido Metallocene. *Organometallics* **2015**, *34*, 3637-3647.

(38) Yang, P.; Zhou, E.; Fang, B.; Hou, G.; Zi, G.; Walter, M. D. Preparation of ($\eta^5$-$C_5Me_5)_2$Th(bipy) and Its Reactivity toward Small Molecules. *Organometallics* **2016**, *35*, 2129-2139.

(39) Ren, W.; Zhou, E.; Fang, B.; Hou, G.; Zi, G.; Fang, D. C.; Walter, M. D. Experimental and Computational Studies on the Reactivity of a Terminal Thorium Imidometallocene towards Organic Azides and Diazoalkanes. *Angew. Chem., Int. Ed.* **2014**, *53*, 11310-11314.

(40) Blake, R. E.; Antonelli, D. M.; Henling, L. M.; Schaefer, W. P.; Hardcastle, K. I.; Bercaw, J. E. A Cationic Imido Complex of Permethyltantalocene: $H_2$ and Carbon-Hydrogen Bond Activation, [2 + 2] Cycloaddition Reactions, and an Unusual Reaction with Carbon Dioxide That Affords Coordinated Isocyanate. *Organometallics* **1998**, *17*, 718-725.

(41) Rocklage, S. M.; Schrock, R. R. Tantalum Imido Complexes. *J. Am. Chem. Soc.* **1980**, *102*, 7809-7811.

(42) Royo, P.; Sánchez-Nieves, J. Oxo and Imido/Imido Exchange and C-H Activation Reactions Based on Pentamethylcylopentadienyl Imido Tantalum Complexes. *J. Organomet. Chem.* **2000**, *597*, 61-68.

(43) Tomson, N. C.; Arnold, J.; Bergman, R. G. Halo, Alkyl, Aryl, and Bis(Imido) Complexes of Niobium Supported by the β-Diketiminato Ligand. *Organometallics* **2010**, *29*, 2926-2942.

(44) Cundari, T. R. Methane Activation by Group VB Bis(imido) Complexes. *Organometallics* **1994**, *13*, 2987-2994.

(45) Kriegel, B. M.; Bergman, R. G.; Arnold, J. Nitrene Metathesis and Catalytic Nitrene Transfer Promoted by Niobium Bis(imido) Complexes. *J. Am. Chem. Soc.* **2016**, *138*, 52-55.

(46) de With, J.; Horton, A. D.; Orpen, A. G. Unusual [2 + 2] Cycloaddition Adducts of an Imidovanadium Complex with Alkynes and Ethene: Conversion to $\eta^3$-1-Azaallyl and Ethenyl Complexes. *Organometallics* **1993**, *12*, 1493-1496.

(47) Tomson, N. C.; Arnold, J.; Bergman, R. G. Synthesis, Characterization, and Reactions of Isolable (β-Diketiminato)Niobium(III) Imido Complexes. *Organometallics* **2010**, *29*, 5010-5025.

(48) Fostvedt, J. I.; Grant, L. N.; Kriegel, B. M.; Obenhuber, A. H.; Lohrey, T. D.; Bergman, R. G.; Arnold, J. 1,2-Addition and Cycloaddition Reactions of Niobium Bis(imido) and Oxo Imido Complexes. *Chem. Sci.* **2020**, *11*, 11613-11632.

(49) Helgert, T. R.; Zhang, X.; Box, H. K.; Denny, J. A.; Valle, H. U.; Oliver, A. G.; Akurathi, G.; Webster, C. E.; Hollis, T. K. Extreme π-Loading as a Design Element for Accessing Imido Ligand Reactivity. A CCC-NHC Pincer Tantalum Bis(Imido) Complex: Synthesis, Characterization, and Catalytic Oxidative Amination of Alkenes. *Organometallics* **2016**, *35*, 3452-3460.

(50) Liang, G.; Hollis, T. K.; Webster, C. E. Computational Analysis of the Intramolecular Oxidative Amination of an Alkene Catalyzed by the Extreme π-Loading *N*-Heterocyclic Carbene Pincer Tantalum(V) Bis(Imido) Complex. *Organometallics* **2018**, *37*, 1671-1681.

(51) Bannwarth, C.; Ehlert, S.; Grimme, S. GFN2-xTB—An Accurate and Broadly Parametrized Self-Consistent Tight-Binding Quantum Chemical Method with Multipole Electrostatics and Density-Dependent Dispersion Contributions. *J. Chem. Theory Comput.* **2019**, *15*, 1652-1671.

(52) Elpitiya, G. R.; Malbrecht, B. J.; Jenkins, D. M. A Chromium(II) Tetracarbene Complex Allows Unprecedented Oxidative Group Transfer. *Inorg. Chem.* **2017**, *56*, 14101-14110.

(53) Lin, K. M.; Wang, P. Y.; Shieh, Y. J.; Chen, H. Z.; Kuo, T. S.; Tsai, Y. C. Reductive N-N Bond Cleavage and Coupling of Organic Azides Mediated by Chromium(I) and Vanadium(I) β-Diketiminate. *New J. Chem.* **2010**, *34*, 1737-1745.

(54) Monillas, W. H.; Yap, G. P. A.; Theopold, K. H. Reactivity of a Low-Valent Chromium Dinitrogen Complex. *Inorganica Chim. Acta* **2011**, *369*, 103-119.

(55) Addison, A. W.; Rao, T. N.; Reedijk, J.; van Rijn, J.; Verschoor, G. C. Synthesis, Structure, and Spectroscopic Properties of Copper(II) Compounds Containing Nitrogen-Sulfur Donor Ligands; the Crystal and Molecular Structure of Aqua[1,7-bis(*N*-methylbenzimidazol-2'-yl)-2,6-dithiaheptane]copper(II) Perchlorate. *J. Chem. Soc., Dalton Trans.* **1984**, 1346-1356.

(56) Kriegel, B. M.; Bergman, R. G.; Arnold, J. Nitrene Metathesis and Catalytic Nitrene Transfer Promoted by Niobium Bis(Imido) Complexes. *J. Am. Chem. Soc.* **2016**, *138*, 52-55.

(57) Bursch, M.; Neugebauer, H.; Grimme, S. Structure Optimisation of Large Transition-Metal Complexes with Extended Tight-Binding Methods. *Angew. Chem., Int. Ed.* **2019**, *58*, 11078-11087.

(58) Bursch, M.; Hansen, A.; Pracht, P.; Kohn, J. T.; Grimme, S. Theoretical Study on Conformational Energies of Transition Metal Complexes. *Phys. Chem. Chem. Phys.* **2021**, *23*, 287-299.

(59) Tantillo, D. J. Recent Excursions to the Borderlands between the Realms of Concerted and Stepwise: Carbocation Cascades in Natural Products Biosynthesis. *J. Phys. Org. Chem.* **2008**, *21*, 561-570.

(60) Tang, J.; Xu, D. H.; Wang, X.; Li, L.; Liu, X. Y.; Su, X. T.; Guo, J.; Zhai, B. A Density Functional Theory Study of the Stereoselectivity of $Cu(OTf)_2$-Catalyzed [3+2] Cycloaddition of Trifluoromethylated *N*-Acylhydrazones and Isoprene: A Concerted Asynchronous Mechanism. *Int. J. Quantum Chem.* **2020**, *120*, 1-11.

(61) Hess, B. A.; Smentek, L. Concerted, Highly Asynchronous, Enzyme-Catalyzed [4 + 2] Cycloaddition in the Biosynthesis of Spinosyn A; Computational Evidence. *Org. Biomol. Chem.* **2012**, *10*, 7503-7509.

(62) Gianetti, T. L.; Nocton, G.; Minasian, S. G.; Tomson, N. C.; Kilcoyne, A. L. D.; Kozimor, S. A.; Shuh, D. K.; Tyliszczak, T.; Bergman, R. G.; Arnold, J. Diniobium Inverted Sandwich Complexes with $\mu$-$\eta^6$:$\eta^6$-Arene Ligands: Synthesis, Kinetics of Formation, and Electronic Structure. *J. Am. Chem. Soc.* **2013**, *135*, 3224-3236.

SYNOPSIS. We report two niobatetrazene complexes that can be interconverted upon addition of excess alkyl azide. We propose this azide metathesis transformation proceeds *via* a series of [3+2] and retro-[3+2] cycloaddition reactions and generates two π-loaded bis(imido) intermediates, as evidenced by spectroscopic, crystallographic, and computational studies. Notably, computational studies predict that the individual cycloaddition/retrocycloaddition processes occur *via* an asynchronous concerted mechanism, in which formation of a temporary niobaazacyclopropane moiety punctuates the two bond formation/cleavage events.

TABLE OF CONTENTS GRAPHIC.